Attosecond sublevel beating and nonlinear dressing on the 3d-to-5p and 3p-to-5s core-transitions at 91.3 eV and 210.4 eV in krypton

Enikoe Seres,[1,*] Jozsef Seres,[1] Shinichi Namba,[2] John Afa,[3] and Carles Serrat[3]

[1]*Institute of Atomic and Subatomic Physics - E141, Vienna University of Technology, Stadionallee 2, 1020 Vienna, Austria*
[2]*Graduate School of Engineering, Hiroshima University, 1-4-1 Kagamiyama, Higashi-Hiroshima, Hiroshima 739-8527, Japan*
[3]*Universitat Politècnica de Catalunya, Departament de Física, Colom 11, 08222 Terrassa, Spain*
[*]*enikoe-judit-seres@lycos.com*

Abstract: Applying extreme ultraviolet (XUV) transient absorption spectroscopy, the dynamics of the two laser dressed transitions $3d_{5/2}$-to-$5p_{3/2}$ and $3p_{3/2}$-to-$5s_{1/2}$ at photon energies of 91.3 eV and 210.4 eV were examined with attosecond temporal resolution. The dressing process was modeled with density matrix equations which are found to describe very accurately both the experimentally observed transmission dynamics and the linear and nonlinear dressing oscillations at 0.75 PHz and 1.5 PHz frequencies. Furthermore, using Fourier transform XUV spectroscopy, quantum beats from the $3d_{5/2}$-$3d_{3/2}$ and $3p_{3/2}$-$3p_{1/2}$ sublevels at 0.3 PHz and 2.0 PHz were experimentally identified and resolved.

OCIS codes: (320.7150) Ultrafast spectroscopy; (020.2649) Strong field laser physics; (190.4160) Multiharmonic generation.

References and links

1. M. Wu, S. Chen, S. Camp, K. J. Schafer, and M. B. Gaarde, "Theory of strong- field attosecond transient absorption," J. Phys. B **49**, 062003 (2016).
2. J. Seres, E. Seres, D. Hochhaus, B. Ecker, D. Zimmer, V. Bagnoud, T. Kuehl, and C. Spielmann, "Laser-driven amplification of soft X-rays by parametric stimulated emission in neutral gases," Nat. Phys. **6**, 455–461 (2010).
3. J. Seres, E. Seres, B. Landgraf, B. Ecker, B. Aurand, A. Hoffmann, G. Winkler, S. Namba, T. Kuehl, and C. Spielmann, "Parametric amplification of attosecond pulse trains at 11 nm," Sci. Rep. **4**, 4254 (2014).
4. C. Serrat, D. Roca, J. M. Budesca, J. Seres, E. Seres, B. Aurand, A. Hoffmann, S. Namba, T. Kuehl, and C. Spielmann, "Avalanche of stimulated forward scattering in high harmonic generation," Opt. Express **24**(8), 8028–8044 (2016).
5. E. Seres, J. Seres, and C. Spielmann, "X-ray absorption spectroscopy in the keV range with laser generated high harmonic radiation," Appl. Phys. Lett. **89**, 181919 (2006).
6. T. Popmintchev, M.-C. Chen, D. Popmintchev, P. Arpin, S. Brown, S. Alisauskas, G. Andriukaitis, T. Balciunas, O. D. Mücke, A. Pugzlys, A. Baltuska, B. Shim, S. E. Schrauth, A. Gaeta, C. Hernández-García, L. Plaja, A. Becker, A. Jaron-Becker, M. M. Murnane, and H. C. Kapteyn, "Bright Coherent Ultrahigh Harmonics in the keV X-ray Regime from Mid-Infrared Femtosecond Lasers," Science **336**(6086), 1287–1291 (2012).
7. J. Seres, E. Seres, B. Landgraf, B. Ecker, B. Aurand, T. Kuehl, and C. Spielmann, "High-harmonic generation and parametric amplification in the soft X-rays from extended electron trajectories," Sci. Rep. **4**, 4234 (2014).
8. O. Kwon and D. Kim, "PHz current switching in calcium fluoride single crystal," Appl. Phys. Lett. **108**, 191112 (2016).
9. M. Schultze, K. Ramasesha, C. D. Pemmaraju, S. A. Sato, D. Whitmore, A. Gandman, J. S. Prell, L. J. Borja, D. Prendergast, K. Yabana, D. M. Neumark, and S. R. Leone, "Ultrafast dynamics. Attosecond band-gap dynamics in silicon," Science **346**(6215), 1348–1352 (2014).
10. E. Seres, J. Seres, C. Serrat, and S. Namba, "Core-level attosecond transient absorption spectroscopy of laser-dressed solid films of Si and Zr," Phys. Rev. B **94**, 165125 (2016).
11. M. Lucchini, S. A. Sato, A. Ludwig, J. Herrmann, M. Volkov, L. Kasmi, Y. Shinohara, K. Yabana, L. Gallmann, and U. Keller, "Attosecond dynamical Franz-Keldysh effect in polycrystalline diamond," Science **353**(6302), 916–919 (2016).
12. M. Chini, X. Wang, Y. Cheng, Y. Wu, D. Zhao, D. A. Telnov, S.-I. Chu, and Z. Chang, "Sub-cycle Oscillations in Virtual States Brought to Light," Sci. Rep. **3**, 1105 (2013).

13. M. Reduzzi, J. Hummert, A. Dubrouil, F. Calegari, M. Nisoli, F. Frassetto, L. Poletto, S. Chen, M. Wu, M. B. Gaarde, K. Schafer, and G. Sansone, "Polarization control of absorption of virtual dressed states in helium," Phys. Rev. A **92**, 033408 (2015).
14. E. R. Simpson, A. Sanchez-Gonzalez, D. R. Austin, Z. Diveki, S. E. E. Hutchinson, T. Siegel, M. Ruberti, V. Averbukh, L. Miseikis, C. S. Strüber, L. Chipperfield, and J. P. Marangos, "Polarisation response of delay dependent absorption modulation in strong field dressed helium atoms probed near threshold," New J. Phys. **18**, 083032 (2016).
15. Y. Li, C. Gao, W. Dong, J. Zeng, Z. Zhao, and J. Yuan, "Coherence and resonance effects in the ultra-intense laser-induced ultrafast response of complex atoms," Sci. Rep. **6**, 18529 (2016).
16. X. Wang, M. Chini, Y. Cheng, Y. Wu, X.-M. Tong, and Z. Chang, "Subcycle laser control and quantum interferences in attosecond photoabsorption of neon," Phys. Rev. A **87**, 063413 (2013).
17. Y. Cheng, M. Chini, X. Wang, A. Gonzalez-Castrillo, A. Palacios, L. Argenti, F. Martın, and Z. Chang, "Reconstruction of an excited-state molecular wave packet with attosecond transient absorption spectroscopy," Phys. Rev. A **94**, 023403 (2016).
18. A. N. Pfeiffer and S. R. Leone, "Transmission of an isolated attosecond pulse in a strong-field dressed atom," Phys. Rev. A **85**, 053422 (2012).
19. Y. Kobayashi, H. Timmers, M. Sabbar, S. R. Leone, and D. M. Neumark, "Attosecond transient-absorption dynamics of xenon core-excited states in a strong driving field," Phys. Rev. A **95**, 031401(R) (2017).
20. M. Sabbar, H. Timmers, Y.-J. Chen, A. K. Pymer, Z.-H. Loh, S. G. Sayres, S. Pabst, R. Santra, and S. R. Leone, "State-resolved attosecond reversible and irreversible dynamics in strong optical fields," Nat. Phys. **13**, 472–478 (2017).
21. H. Wang, M. Chini, S. Chen, C.-H. Zhang, F. He, Y. Cheng, Y. Wu, U. Thumm, and Z. Chang, "Attosecond Time-Resolved Autoionization of Argon," Phys. Rev. Lett. **105**(14), 143002 (2010).
22. C. Ott, A. Kaldun, L. Argenti, P. Raith, K. Meyer, M. Laux, Y. Zhang, A. Blättermann, S. Hagstotz, T. Ding, R. Heck, J. Madroñero, F. Martín, and T. Pfeifer, "Reconstruction and control of a time-dependent two-electron wave packet," Nature **516**(7531), 374–378 (2014).
23. E. Goulielmakis, Z.-H. Loh, A. Wirth, R. Santra, N. Rohringer, V. S. Yakovlev, S. Zherebtsov, T. Pfeifer, A. M. Azzeer, M. F. Kling, S. R. Leone, and F. Krausz, "Real-time observation of valence electron motion," Nature **466**(7307), 739–743 (2010).
24. E. R. Hosler and S. R. Leone, "Characterization of vibrational wave packets by core-level high-harmonic transient absorption spectroscopy," Phys. Rev. A **88**, 023420 (2013).
25. A. R. Attar, A. Bhattacherjee, C. D. Pemmaraju, K. Schnorr, K. D. Closser, D. Prendergast, and S. R. Leone, "Femtosecond x-ray spectroscopy of an electrocyclic ring-opening reaction," Science **356**(6333), 54–59 (2017).
26. Y. Pertot, C. Schmidt, M. Matthews, A. Chauvet, M. Huppert, V. Svoboda, A. von Conta, A. Tehlar, D. Baykusheva, J.-P. Wolf, and H. J. Wörner, "Time-resolved x-ray absorption spectroscopy with a water window high-harmonic source," Science **355**(6322), 264–267 (2017).
27. E. Seres and C. Spielmann, "Ultrafast soft x-ray absorption spectroscopy with sub-20-fs resolution," Appl. Phys. Lett. **91**, 121919 (2007).
28. E. Seres and C. Spielmann, "Time-resolved optical pump X-ray absorption probe spectroscopy in the range up to 1 keV with 20 fs resolution," J. Mod. Opt. **55**(16), 2643–2651 (2008).
29. E. Seres, J. Seres, and C. Spielmann, "Time resolved spectroscopy with femtosecond soft-x-ray pulses," Appl. Phys., A Mater. Sci. Process. **96**, 43–50 (2009).
30. G. C. King, M. Tronct, F. H. Read, and R. C. Bradford, "An investigation of the structure near the $L_{2,3}$ edges of argon, the $M_{4,5}$ edges of krypton and the $N_{4,5}$ edges of xenon, using electron impact with high resolution," J. Phys. B **10**(12), 2479–2495 (1977).
31. O. Sairanen, A. Kivimäki, E. Nõmmiste, H. Aksela, and S. Aksela, "High-resolution pre-edge structure in the inner-shell ionization threshold region of rare gases Xe, Kr, and Ar," Phys. Rev. A **54**(4), 2834–2839 (1996).
32. J. Lang and W. S. Watson, "The photoabsorption coefficients of krypton and xenon from 48 Å to 210 Å," J. Phys. B **8**(14), L339–L343 (1975).
33. J. B. West and G. V. Marr, "The absolute photoionization cross sections of helium, neon, argon and krypton in the extreme vacuum ultraviolet region of the spectrum," Proc. R. Soc. Lond. A Math. Phys. Sci. **349**, 397–421 (1976).
34. B. L. Henke, E. M. Gullikson, and J. C. Davis, "X-ray interactions: photoabsorption, scattering, transmission, and reflection at E=50-30000 eV, Z=1-92," At. Data Nucl. Data Tables **54**(2), 181–342 (1993).
35. M.-F. Lin, A. N. Pfeiffer, D. M. Neumark, S. R. Leone, and O. Gessner, "Strong-field induced XUV transmission and multiplet splitting in 4d-16p core-excited Xe studied by femtosecond XUV transient absorption spectroscopy," J. Chem. Phys. **137**(24), 244305 (2012).
36. I. J. Afa and C. Serrat, "Quantum Control of Population Transfer and Vibrational States via Chirped Pulses in Four Level Density Matrix Equations," Appl. Sci. **6**, 351 (2016).
37. M. B. Gaarde, C. Buth, J. L. Tate, and K. J. Schafer, "Transient absorption and reshaping of ultrafast XUV light by laser-dressed helium," Phys. Rev. A **83**, 013419 (2011).
38. J. Herrmann, M. Weger, R. Locher, M. Sabbar, P. Riviere, U. Saalmann, J.-M. Rost, L. Gallmann, and U. Keller, "Virtual single-photon transition interrupted: Time-gated optical gain and loss," Phys. Rev. A **88**, 043843 (2013).

39. D. Bauer and P. Mulser, "Exact field ionization rates in the barrier-suppression regime from numerical time-dependent Schrodinger-equation calculations," Phys. Rev. A **59**, 569–577 (1999).
40. Y. Kobayashi, N. Hirayama, A. Ozawa, T. Sukegawa, T. Seki, Y. Kuramoto, and S. Watanabe, "10-MHz, Yb-fiber chirped-pulse amplifier system with large-scale transmission gratings," Opt. Express **21**(10), 12865–12873 (2013).

1. Introduction

Intense laser fields interact with atoms, molecules and even solids non-adiabatically by producing transient changes in their occupied or unoccupied electronic quantum states. The response of the material to this so called dressing is typically very fast lying in the few PHz and sub-PHz frequency range. Attosecond transient absorption spectroscopy (ATAS) [1] is a suitable spectroscopy tool to follow and study such a fast material responses. Revealing PHz-scale responses of materials helps us to develop and improve coherent extreme ultraviolet (XUV) [2–4] and soft X-ray (SXR) [5–7] light sources by means of high harmonic generation (HHG) and to extend the operational speed of different optoelectronic detectors [8].

Nowadays, ATAS is extensively applied to study intense laser field dressed solids like Si [9, 10], diamond [11], Zr [10], by probing valence or core electrons. Gases like helium [12–15], neon [16] and H_2 [17] were mainly probed by their valence electrons at around and below 20 eV with attosecond or femtosecond resolution. Probing core level electronic states in atoms or molecules is more challenging because they require HHG sources with much higher photon energies, where the conversion efficiency of HHG is typically low. Consequently, mainly xenon gas [18–20], argon [21] and two-electron transitions in He [22] have been studied at around 60 eV, and time resolved spectroscopy at higher photon energies were rare [23–26] and gave mainly femtosecond resolution even in solids [27–29].

Our aim was to measure the time-resolved XUV absorption of neutral krypton gas. ATAS of krypton was earlier measured [23] at its ionized states. In the case of neutral krypton, a strong absorption can be observed between 90 and 95 eV containing several transitions between the occupied 3d inner-shell and the unoccupied np levels [30, 31], and transitions from the 3p inner-shell at around 210 eV have also been measured and predicted [32–34].

The generated HHG spectrum that we used as probe covered the spectral range from 70 eV to 230 eV, making it possible to study both types of core level transitions i.e. the excitations from the sublevels of the 3d and 3p electronic states. The study of these transitions in Kr was motivated by the fact that the distance between the 5s and 5p levels is 1.52 eV, which is within the bandwidth of our dressing laser pulse (central energy was at 1.55 eV). Consequently, the 5s and 5p levels were resonantly coupled by the dressing laser field and a strong dressing effect was predicted for both the $3d_{5/2}$-to-$5p_{3/2}$ and $3p_{3/2}$-to-$5s_{1/2}$ transitions at 91.3 eV and 210.4 eV, respectively. Furthermore, since the 5p and 6p levels have an energy-difference of 1.3 eV, it was also close to resonance with the laser field.

2. Experimental setup and examined transitions of krypton

In the experimental arrangement, similarly to our earlier measurement [10], a concentric mirror-pair focused the 25-fs-long, 200 mJ pulses of a 10 Hz Ti:sapphire laser system to two gas sources, see Fig. 1(a). The inner mirror focused the 6 mJ/pulse portion of the laser beam to a jet containing Ne gas for HHG serving as probe pulse. The beam diameter in the focus was 110 μm giving a peak intensity of about 1.5×10^{15} W/cm^2 expecting Gaussian pulse shape, a suitably large one to produce harmonics up to the cut-off energy of about 300 eV. Zr thin-film filter was placed before the XUV spectrograph (McPherson 248/310G with multichannel plate) to suppress all light completely below 50 eV. The gas jet was a tube with diameter of 1 mm to block as little portion of the laser beam from the outer mirror as possible and it was drilled through for the laser beam focused by the inner mirror. The generated harmonic spectrum covered a wide spectral range from about 70 eV to 230 eV, Fig. 1(b), at the optimal backing pressure of the Ne gas of 1.6 bar. Harmonic lines at different parts of the spectrum are well recognizable. For calibration purpose, 100-nm-thick Si foil was used in the

measurements when it is not stated otherwise, of which L-edge can be seen in Fig. 1(b) at about 100 eV.

The generated divergent HHG beam passed through the 1 mm diameter drilled holes of the second gas jet (tube with 3 mm diameter) placed 500 mm from the HHG source. This contained the examined Kr gas and the HHG beam probed the transmission change in Kr produced by the dressing laser field. For dressing/pump, the outer mirror focused a conical beam to the Kr gas. In the focus, the outer mirror produced a ring structure. The laser energy reaching the outer mirror was controlled with a motorized aperture between 12 and 50 mJ giving laser peak intensities in the Kr gas between 4×10^{13} and 6×10^{14} W/cm^2 estimated from the beam profile and pulse energy. Measurable HHG was not observed from Kr. Using a suitable distance between the gas jets, the intensity originated from the divergent laser beam of the inner mirror added less than 2% to the dressing intensity, what was negligible as will be discussed later in 4.2.2. The internal movable mirror allowed scanning the delay between the generated harmonic pulses and the dressing laser beam. A BBO crystal between the two gas jets and sum-frequency generation between the pump and probe beam was used to determine the position of the zero delay.

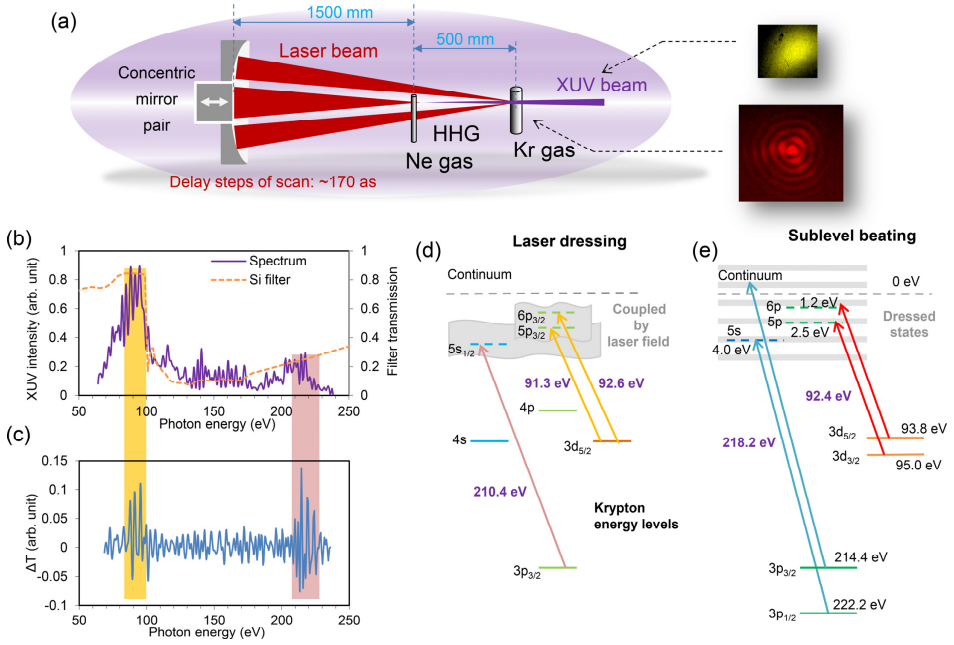

Fig. 1. (a) In the experimental setup, a concentric mirror pair focused the inner and outer parts of the laser beam to two longitudinally separated gas jets, the first used to generate the HHG probe beam and the second used to perform pump/probe measurement of Kr. The insets show the measured beam profiles of the XUV beam and pump laser beam. (b) The high harmonic spectrum generated for probe covered the spectral range from about 70 eV to 230 eV. (c) The average transmission change (ΔT) along a delay scan shows the two spectral ranges where the effect on the Kr gas was observed, namely between 85 and 100 eV and 205-230 eV. (d) Within these spectral ranges two laser dressed transitions: the transition from $3p_{3/2}$ to the dressed $5s_{1/2}$ at 210.4 eV and the transition from $3d_{5/2}$ to the dressed $5p_{3/2}$ at 91.3 eV furthermore (e) beating between 3p and 3d sublevels were examined. The few occupied (solid lines) and unoccupied (dashed lines) states of the krypton atom being within our interest are given.

The generated harmonic spectrum was well suitable to probe the two laser-dressed transitions in Kr gas presented in Fig. 1(d) or the sublevel beating presented in Fig. 1(e). The backing pressure of Kr was chosen to 1.2 bar to be mainly transparent but to produce measurable absorption at the two transitions $3d^{-1}5p$ at 91.3 eV and $3p^{-1}5s$ at 210.4 eV [31, 34]. In the interaction volume we had few torr × cm estimated pressure-length product

(proportional to gas density). The transmission change along a delay scan was averaged in Fig. 1(c) to determine and demonstrate the spectral ranges where laser dressing and beating took effect. Well distinguished changes can be observed in the spectral range of 85-100 eV and 205-230 eV, around the two particular transitions. Some weaker change can also be observed between the two spectral ranges, which can be attributed to the effect of the laser dressing to the 3d to continuum transitions and is out of the interest of the present study.

In the experiment, an attosecond pulse train (APT) was used to probe transient absorption. Since the probe pulses are weak, i.e. the absorption can be considered as linear (no saturation of absorption), and the temporal distance between the pulses in the APT is uniform, APT is suitable for attosecond pump-probe measurements. It can measure processes with time constant shorter than the optical half-cycle or longer than the optical pulse, what was within the scope of our measurements.

3. Beating between 3p and 3d sublevels in krypton

Beating can be expected when two transitions are possible at the same time with close photon energies. As presented in Fig. 1(e), two beating channels are possible in the spectral range of this study: between the $3d_{3/2}$ and $3d_{1/2}$ sublevels and between the $3p_{1/2}$ and $3p_{3/2}$ sublevels. In the case of 3d shell, the distance between the two sublevels is 1.2 eV, which means a beat frequency of $2\nu_B = \Delta E/h$ = 0.29 PHz, what is within the ± 0.02 PHz measurement accuracy of the observed 0.3 PHz frequency. Because the 1.3 eV distance between 5p and 6p levels was almost the same as the distance between the 3d sublevels, the transitions $3d_{1/2} - 5p_{3/2}$ and $3d_{3/2} - 6p_{1/2}$ and their dressed levels were probed at the same time giving one of the possible channels of beating, which had to appear periodically in the spectrum. This channel is noted with red arrows in Fig. 1(e). The other possible beating channel was the transitions from both sublevels into the continuum, and the associated beating had to appear continuously above 95 eV.

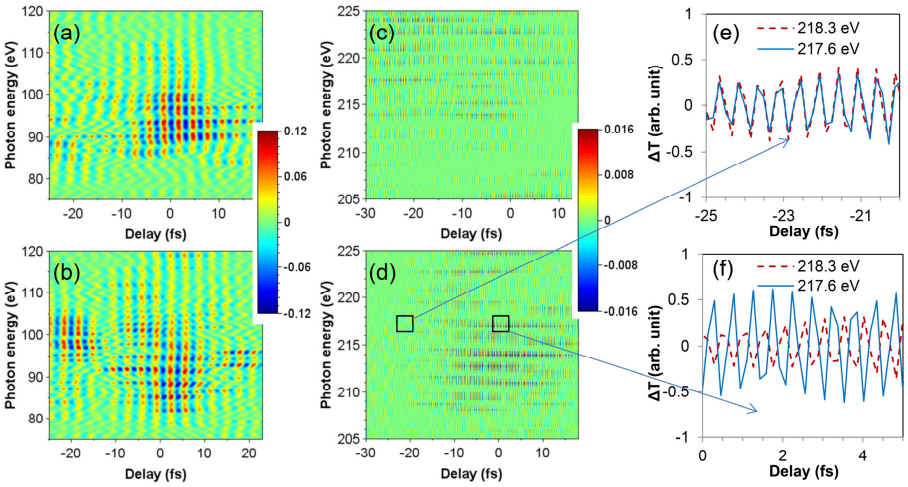

Fig. 2. Beat signals were calculated from the measurements by applying a Fourier window on the (a), (b) 0.3 PHz beat frequency in the case of 3d levels and (c), (d) on the 2 PHz beat frequency for 3p levels at laser intensities of (a), (c) 4×10^{13} W/cm^2 and (b), (d) 8×10^{13} W/cm^2. In panels (e) and (f), the delay dependence of the transmission changes were compared at two nearby photon energies at the $3p_{1/2} - 5s_{-1/2}$ transition at around 218.2 eV.

Similar beating channels should be observed in the case of the 3p level, where the distance between the sublevels is 7.8 eV, giving a beat frequency of $2\nu_B$ = 1.9 PHz that is very close to the observed 2 PHz peak, which gave an 8.2 eV measured difference between the sublevels. We have to note that from the available literature [32–34] the origin and the

accuracy of these level-energies cannot be concluded. The possible channel of the beating from the 3p levels is presented in Fig. 1(e) with blue arrows. Similarly to the 3d level, the beating should give a spectrally periodic pattern produced by the transitions $3p_{1/2}$ - $5s_{-1/2}$ at 218.2 eV and its dressed levels, and by the transition from $3p_{3/2}$ to the continuum. Similarly to 3d shell, another possible channel was the transition from the 3p sublevels to the continuum, what should give a spectrally non-periodic beating pattern beyond 222 eV.

To observe the beating and separate it from other processes, the delay dependent signal was Fourier transformed and Fourier filters were applied to the measured data sets with a window selecting only the 0.3 PHz peak in the case of 3d levels and the 2 PHz peak for 3p levels. More details about the Fourier filtering will be given in Section 4 and Fig. 5. The results can be seen in Figs. 2(a)-2(d) for dressing laser intensities of (a), (c) 4×10^{13} W/cm^2 and (b), (d) 8×10^{13} W/cm^2. In the case of 3d levels, Fig. 2(a) and 2(b), the beating was very well visible and appeared mainly between −10 fs and + 10 fs delays, where the laser intensity was the highest and the spectral periodicity can be observed for both intensities. At the higher intensity, the beating spread over a boarder spectral range, as it can be expected, while the higher laser intensity produced more high-order dressed levels. The continuous beating contribution can mainly be seen between −20 fs and −10 fs delay at around 100 eV, where there was no periodic beating. In the case of 3p levels, Fig. 2(c) and 2(d), the beating was relatively weak at lower laser intensity Fig. 2(c) and appeared mainly at higher photon energies and the continuous contribution dominated. However, at higher intensity Fig. 2(d), it was spectrally periodic and it appeared in the −10 fs to + 10 fs delay range, as it was expected. More details were resolved at the $3p_{1/2} - 5s_{-1/2}$ transition at around 218.2 eV. The black frames in Fig. 2(d) show the delay ranges where transmissions were plotted separately in Figs. 2(e) and 2(f) and at two neighbor photon energies just below and above the transition. Figure 2(e) shows the XUV transmission at negative delay before strong dressing. Here, the beatings were weak and in phase. At around zero delay in Fig. 2(f), where the laser intensity and consequently the dressing and beating were strong, the phase between the two photon energies changed to inverse. To understand fully the detailed behavior of the beating, development of a suitable theoretical model and further examinations are needed.

4. Dynamics of laser dressing in krypton

As presented in Fig. 1(d), two types of possible core transition can be studied by the broad HHG spectrum that was generated, namely the $3d_{5/2}$-to-$5p_{3/2}$ and $3p_{3/2}$-to-$5s_{1/2}$ transitions at 91.3 eV and 210.4 eV, respectively. The energy difference between the $5s_{1/2}$ and $5p_{3/2}$ levels of Kr is 1.52 eV, which gave us a unique opportunity to couple these levels resonantly with short Ti:sapphire laser pulses, and due to this coupling a strong dressing effect was expected. We studied it theoretically and experimentally.

4.1. Theoretical predictions of the laser dressing on the XUV transmissions

To make predictions about the expected effect of the laser dressing and for comparison with measurements, calculations were performed. Density matrix equations were used beyond the rotating wave approximation (RWA), since this approximation is unsuitable when the field strength of the control IR field is in the high-field regime [35]. To follow the processes for the $3d^{-1}5p$ transition, 4 levels were taken into account, namely 3d, 5s, 5p, and 6p. Note that the $3d^{-1}6p$ (92.6 eV) transition was included in the calculation since it is close to one of the dressed states of $3d^{-1}5p$, as mentioned above. The four-level system equations correspond to a double-Λ configuration [36] and they read

$$
\begin{aligned}
\dot{\rho}_{22} &= -i\bar{E}\left[\mu_{23}\left(\rho_{23}-\rho_{32}\right)+\mu_{24}\left(\rho_{24}-\rho_{42}\right)\right] \\
\dot{\rho}_{33} &= i\bar{E}\left[\mu_{13}\left(\rho_{13}-\rho_{31}\right)+\mu_{23}\left(\rho_{23}-\rho_{32}\right)\right] \\
\dot{\rho}_{44} &= i\bar{E}\left[\mu_{14}\left(\rho_{14}-\rho_{41}\right)+\mu_{24}\left(\rho_{24}-\rho_{42}\right)\right] \\
\dot{\rho}_{11} &= -\dot{\rho}_{22}-\dot{\rho}_{33}-\dot{\rho}_{44} \\
\dot{\rho}_{12} &= i\omega_{12}\rho_{12}+i\bar{E}\left[\mu_{13}\rho_{32}-\mu_{23}\rho_{13}+\mu_{14}\rho_{42}-\mu_{24}\rho_{14}\right] \\
\dot{\rho}_{13} &= i\omega_{13}\rho_{13}+i\bar{E}\left[\mu_{13}\left(\rho_{33}-\rho_{11}\right)+\mu_{14}\rho_{43}-\mu_{23}\rho_{12}\right] \\
\dot{\rho}_{14} &= i\omega_{14}\rho_{14}+i\bar{E}\left[\mu_{14}\left(\rho_{44}-\rho_{11}\right)+\mu_{24}\rho_{12}-\mu_{13}\rho_{34}\right] \\
\dot{\rho}_{23} &= i\omega_{23}\rho_{23}+i\bar{E}\left[\mu_{23}\left(\rho_{33}-\rho_{22}\right)+\mu_{24}\rho_{43}-\mu_{13}\rho_{21}\right] \\
\dot{\rho}_{24} &= i\omega_{24}\rho_{24}+i\bar{E}\left[\mu_{24}\left(\rho_{44}-\rho_{22}\right)+\mu_{23}\rho_{34}-\mu_{14}\rho_{21}\right] \\
\dot{\rho}_{34} &= i\omega_{34}\rho_{34}+i\bar{E}\left[\mu_{13}\rho_{14}-\mu_{14}\rho_{31}+\mu_{23}\rho_{24}-\mu_{24}\rho_{32}\right]
\end{aligned}
\tag{1}
$$

where ρ_{ii} are the populations of levels i, with i = 1, 2, 3, 4 corresponding to levels 3d, 5s, 5p, 6p, respectively, the off-diagonal elements ρ_{ij}, with $\rho_{ji}=\rho_{ij}^{*}$, represent the coherences between levels i, j, μ_{ij} are the dipole coupling coefficients of the corresponding transitions and ω_{ij} are their angular frequencies. For the $3p^{-1}5s$ transition, a corresponding three-level system in a cascade configuration 3p-5s-5p was considered. The laser pulses are of Gaussian shape, with the electric field $E=\hbar\bar{E}$ given by

$$
E(t)=E_{IR}e^{-2\ln 2(t/t_{IR})^{2}}\cos(\omega_{IR}t)+E_{XUV}e^{-2\ln 2[(t-t_{0})/t_{XUV}]^{2}}\cos\left[\omega_{XUV}(t-t_{0})\right] \tag{2}
$$

where E_{IR} and E_{XUV} are the peak amplitudes of the IR and XUV pulses, respectively, ω_{IR} and ω_{XUV} are their optical angular frequencies. The duration of the pulses: t_{IR} and t_{XUV} are the full width at half maximum (FWHM) of the pulse intensity profiles. t_0 is the delay between the IR and the XUV pulses. The values of the parameters considered in the simulations shown in Fig. 2 are: $\mu_{13}=\mu_{14}=7\times10^{-32}$ Cm, $\mu_{23}=\mu_{24}=2.1\times10^{-29}$ Cm, ω_{12} = 89.8 eV, ω_{23} = 1.5 eV, ω_{34} = 1.3 eV, and ω_{XUV} = 91.95 eV, for the $3d^{-1}5p$ four-level system (upper row in Fig. 3); and $\mu_{12}=3.3\times10^{-32}$ Cm, $\mu_{23}=3.0\times10^{-29}$ Cm, ω_{12} = 210.4 eV, ω_{23} = 1.5 eV, and ω_{XUV} = 210.4 eV, for the $3p^{-1}5s$ three-level system (lower row in Fig. 3). ω_{IR} = 1.55 eV t_{IR} = 25 fs, t_{XUV} = 200 as, the peak intensity of the XUV pulse is $I_{XUV}=10^{8}$ W/cm^2, and t_0 is considered from −80 fs to 80 fs in steps of 0.2 fs. The atomic polarization response is

$$
P=2\left[\mu_{13}\,\mathrm{Re}\left(\rho_{13}\right)+\mu_{14}\,\mathrm{Re}\left(\rho_{14}\right)\right]. \tag{3}
$$

For the calculation of the time evolution of the atomic polarization, we subtract the contribution from the IR field alone, and we safely use a window function given by a super Gaussian centered at the IR pulse with a width of 40 fs (FWHM) in order to avoid the coherences induced by the XUV pulse and the upper states when the atom is not laser dressed, which in the numerical simulation produces a “ringing” effect until long after the XUV pulse is over [37]. This well-known spurious ringing does not produce stimulated emission or absorption and is basically absent when the atom is laser dressed. The calculated transmission signal is given by

$$
T=\exp\left[-\tfrac{4\pi\omega NL}{c}\,\mathrm{Im}\left(\tfrac{\tilde{P}(\omega)}{\tilde{E}_{XUV}(\omega)}\right)\right], \tag{4}
$$

where $\tilde{P}(\omega)$ and $\tilde{E}_{XUV}(\omega)$ are the spectra of the atomic polarization and the input XUV field, respectively, c is the speed of light in vacuum, N is the atomic density, and L is the length of the interaction region [35]. In the simulations we chose NL = 9×10^{21} m^{-2}, which corresponds to a pressure of 120 mbar at room temperature with a propagation distance of 3 mm.

Calculations were performed in a wide intensity range from $I_{IR} = 4 \times 10^{13}$ W/cm^2 to 6×10^{14} W/cm^2 for both the $3d^{-1}5p$ (91.3 eV) and $3p^{-1}5s$ (210.4 eV) transitions and three of them are shown in Fig. 3, where *T-1* is plotted as a function of delay and photon energy. The unique feature of Kr that the energy distance between the 5s and 5p levels is 1.52 eV indeed assures a strong dressing effect for both the $3d^{-1}5p$ and the $3p^{-1}5s$ transitions. As can be seen from the calculations in Fig. 3, the absorption lines of $3d^{-1}5p$, $3d^{-1}6p$ Figs. 3(a)-3(c) and $3p^{-1}5s$ Figs. 3(d)-3(f) split to a structure of absorption between the delays of –20 fs and + 20 fs, when the gas is pumped by the dressing laser pulse. It means temporal absorption at other photon energies than the original absorption lines appeared. This structure was broader at higher intensities and there was a spectrally periodic structure with the energy of the pump laser photons. This structure is almost washed out and disappears at very high intensities between –40 and + 40 fs. Furthermore, there is a fast oscillation in the absorption following the shape of the square of the electric field of the dressing laser pulse. It can also be seen that the transmission (*T-1*) can exceed 0 meaning the appearance of gain within very short time intervals as was earlier predicted and measured [38]. The calculated dressing effect was about 3-times stronger for the $3d^{-1}5p$ than for the $3p^{-1}5s$ as can be seen from the color bars in Fig. 3.

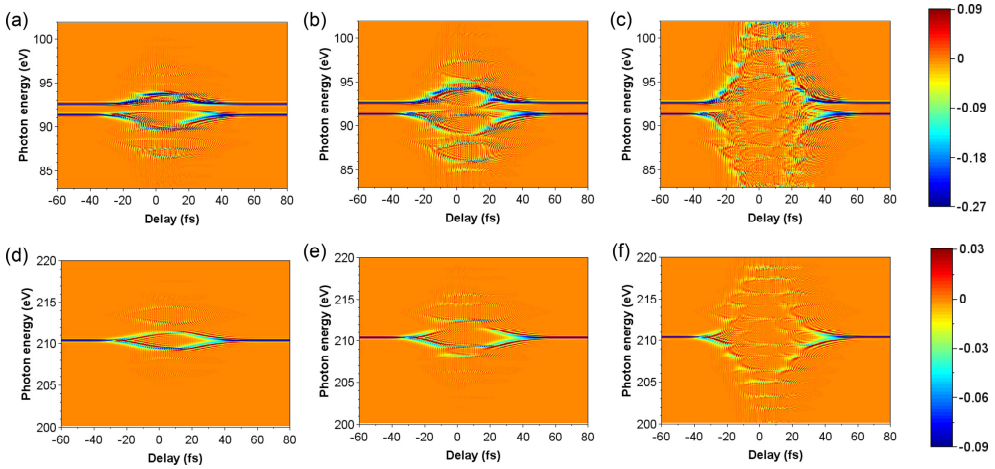

Fig. 3. Calculated XUV transmission change [*T-1*, see Eq. (4)] of the (upper row) $3d^{-1}5p$ and (lower row) $3p^{-1}5s$ dressed transitions at intensities of (a, d) 4×10^{13}, (b, e) 1×10^{14} and (c, f) 6×10^{14} W/cm^2.

4.2. Results on the laser dressing of the $3d^{-1}5p$ and $3p^{-1}5s$ transition of krypton atoms

To examine and resolve the dynamics of the laser dressing on the $3d^{-1}5p$ and $3p^{-1}5s$ transitions of Kr atoms, delay scans were performed with femtosecond resolution in a delay interval of 420 fs using delay steps of 1.4 fs, furthermore with attosecond resolution in a delay interval of 50 fs using delay steps of about 170 as, respectively. Within one delay scan, HHG spectra were recorded with 2 s integration time (20 laser shots) in 300 delay steps limited by technical reasons. According to the calculations (Fig. 3), weak dressing was predicted for a weak driving field below 1×10^{14} W/cm^2, where the ionized fraction of Kr atoms was also small below 10^{-4} according to ionization theories [39] and measurements [40]. In a strong driving field, e.g. at 6×10^{14} W/cm^2, Figs. 3(c), 3(f), the theory predicted a strong dressing

effect on the transmitted XUV signal with all atomic states merged into a continuum. Although for these laser intensities the ionization was strong and almost all the atoms became ionized during the interaction with the laser pulse, as an earlier study on Xe [20] also showed, the dressing effect remained still observable.

4.2.1. Femtosecond dynamics of the transient absorption

Applying a strong field dressing with laser peak intensity of 6×10^{14} W/cm^2, a delay scan was performed with femtosecond (1.4 fs) temporal resolution and plotted in Figs. 4(a) and 4(c) in the spectral ranges around the core transitions of $3p^{-1}5s$ (210.4 eV) and $3d^{-1}5p$ (91.3 eV), respectively. Below the 214.4 eV ($3p_{3/2}$) ionization threshold in Fig. 4(a), strong distortion of the harmonic line H137 at 211 eV can be observed at around zero delay as the consequence of the dressing laser field, as it would be expected from the calculation in Fig. 3(f). Going further from the $3p^{-1}5s$ absorption line, calculations predicted decreasing dressing effects, which was well observable on the measurement. While the harmonic line H135 at 208 eV was still strongly affected, H133 was only weakly and H131 was almost not affected. Above 215 eV (H139, H141), the effect of dressing was not visible in the experiments similarly to [20] probably because this energy range was above the ionization threshold, what was not considered in the theory. In Fig. 4(b), the measured and calculated transient transmissions were compared at two particular photon energies of 210.4 eV, which belonged to the $3p^{-1}5s$ transition, and of 209.3 eV, where the calculations predicted a strong dressing effect. At the $3p^{-1}5s$ absorption line, the calculated strong increase of the transmission was well followed by the measurement. Similarly, the transient absorption at 209.3 eV was well reproduced by the measurement. The fast modulations observable on the calculations were caused by the dressing laser field and had a period of 1.3 fs, which could not be resolved with the 1.4 fs temporal steps of these measurement series. They would have produced only confusing noise in the measurement, so a Fourier filter was applied to suppress the faster than 10 fs processes.

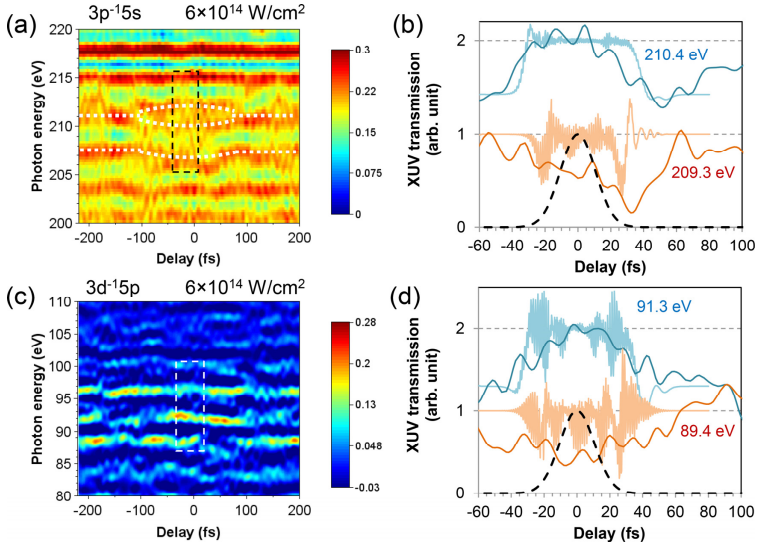

Fig. 4. Femtosecond dynamics of the dressed Kr was resolved at laser intensity of 6×10^{14} W/cm^2. The measurements showed strong transmission change around zero delay at the core transitions of (a) $3p^{-1}5s$ at 210.4 eV noted with white dashed lines, (c) at $3d^{-1}5p$ and $3d^{-1}6p$ transitions between 91.3 eV and 92.6 eV. The dashed frames show the windows where higher resolution measurements were performed. (b), (d) Comparison of the theoretical calculations (thin lines) with the measurements (thick lines) gave good agreement for both spectral ranges. The curves were shifted vertically for better visibility. Black dashed lines note the shape of the laser pulse used for the calculations. The measured transmission changes are given in arbitrary unit in this and every later figure.

The change in the absorption spectrum at around 92 eV during the illumination with the strong laser field was also measured for the transitions $3d^{-1}5p$ and $3d^{-1}6p$ in Fig. 4(c). In this spectral range, the shape of the HHG spectra and especially the presence of the harmonic line would dominate and overwhelm the dressing effect. To avoid this, a Fourier filter had to be applied on the measured spectra to filter out the harmonic line structure at the 0.5 harmonic orders and also the spectral shape at zero order. Consequently, this figure shows only the change of the XUV transmission. Such filtering for Fig. 4(a) was not necessary, because there were no big changes in the spectral shape and the harmonic-line-structure was also weak in that spectral range. In Fig. 4(c), an essential transmission change can be observed at three photon energies, at around 89 eV, 92 eV and 96 eV. At about 92 eV, the transmission increased at around zero delay, which can be attributed to the disappearance of the absorption of the transitions $3d^{-1}5p$ and $3d^{-1}6p$, similarly to the $3p^{-1}5s$ absorption line. This increased transmission was also predicted by simulations at 91.3 eV plotted in Fig. 3(c). The fast modulations observable on the calculations were caused by the dressing laser field, which could not be resolved in the measurements with such a large delay steps. The observed signal at about 89 eV had a strong transmission at negative delays and transient absorption within a time interval at and after zero delays. It can be attributed to a dressed state and also to an additional process of transient two-photon (XUV + NIR) excitation of the $3d^{-1}5s$ transition. In Fig. 4(d), the measurement showed a change of transmission similar to the calculation but within somewhat broader delay range. This difference can be the consequence of the used super-Gaussian temporal window in the calculation making calculations more efficient in the attosecond time scale but less accurate in the sub-ps time scale. The observed signal at 96 eV, which appeared at the ionization threshold, was probably caused by the laser field enhanced ionization, which process was not part of the present study and was not considered in the theory. Both in Figs. 4(a) and 4(c), weaker distortions of the transmitted signal were observed at around ± 190 fs delays, which were probably the consequence of a weaker pre and post pulses in the laser pulse, unrecognized during pulse characterization.

4.2.2. Fourier-transform spectroscopy to recognize attosecond transient processes

Transient changes of two core-level transitions were studied, namely, the transition from $3d_{5/2}$ to $5p_{3/2}$ at around 90 eV and the transition from $3p_{3/2}$ to $5s_{1/2}$ at around 210 eV. Looking into the results of the measurements and calculations in more detail, however, one can recognize different contributions. To do so, measurement series in the time window noted in Fig. 4(a) and 4(c) were performed with attosecond resolution and the 2D data sets (spectrum in harmonic order versus delay) of both the measurements Figs. 7(a), 7(c), 8(b), 8(d) and calculations Fig. 3 were Fourier transformed and compared in Fig. 5. In the first row of Figs. 5(a) and 5(b) show the result of the theory and the second row the results of the corresponding measurements.

A similar change of the transient absorption can be expected in gases as was observed in our earlier measurement for solids [10] and was described as follows

$$\Delta T \propto I_0(\tau)\cos^2(2\pi\nu_0\tau)\cos^4\left(2\pi\nu_B\tau\right), \tag{5}$$

where τ is the delay between the pump and probe pulses; $I_0(\tau)$ is the envelope of the laser pulse; ν_0 is the laser frequency and $\nu_B = \Delta E/2h$ is the beat frequency determined by the energy difference of the sublevels of certain electron shell of the atom. This equation can be rewritten into a more intuitive form

$$\Delta T \propto I_0(\tau)\left[1+\cos(4\pi\nu_0\tau)\right]\left[3+4\cos\left(4\pi\nu_B\tau\right)+\cos\left(8\pi\nu_B\tau\right)\right]. \tag{6}$$

It predicts laser dressing at $2\nu_0$ = 0.75 PHz, beating at frequencies $2\nu_B$ and $4\nu_B$, furthermore few smaller mixed terms. One can recognize from the calculations in Fig. 5 that

the density matrix Eqs. (1) describe the dressing as a strongly nonlinear process and beyond the expected dressing frequency of 0.75 PHz, its second and even third harmonics appear at $4\nu_0$ = 1.5 PHz and $6\nu_0$ = 2.25 PHz. The linear description Eq. (6) however, did not predict the appearance of $4\nu_0$ and $6\nu_0$ harmonics of the laser dressing. In comparison to the 1D Fourier spectra of the measurements Fig. 5(c) and 5(d), the peaks at 0.75 PHz and 1.5 PHz clearly appeared and were noted with black arrows. Mainly in Fig. 5(d), the measured dressing peaks were double peaks of 0.65/0.75 PHz and their harmonics of 1.3/1.5 PHz. The third harmonic peaks at 1.95/2.25 PHz can even be recognized but they were near the level of the background noise. The origin of the double-peek structure has not still been resolved.

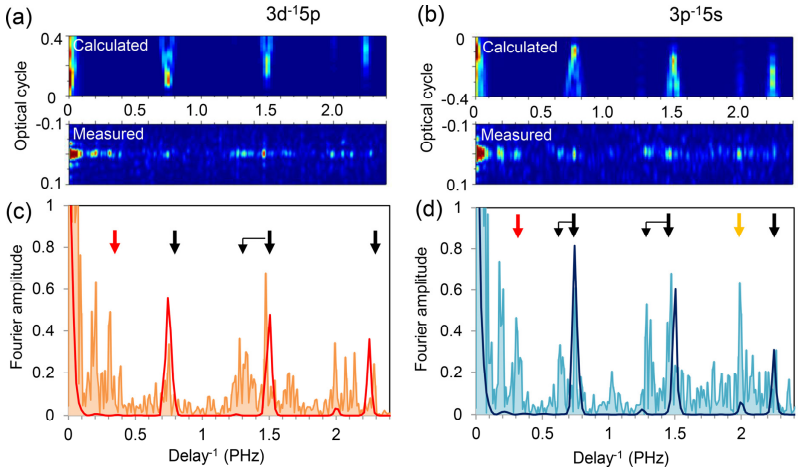

Fig. 5. (a), (b) The 2D Fourier transform of the modelled and the measured 2D spectra-delay data sets (normalized), for the (a), (c) $3d^{-1}5p$ and (b), (d) $3p^{-1}5s$ transitions, show the peaks of the laser (black arrows) dressing and (yellow arrow) the beating. (c), (d) Averaged Fourier spectra of the (orange/light-blue) measurement and (red/blue) calculation. Possible transitions are noted with arrows where beating can be observed from 3d and 3p levels, respectively.

Additional strong spectral components can be observed at 2 PHz in Fig. 5(d) noted with yellow arrow and at 0.3 PHz in both Fig. 5(c) and 5(d) noted with red arrows. These two peaks were the beating between two absorption channels starting from the sublevels of the 3d and 3p quantum states of Kr and the possible beating schemes were presented in Fig. 1(e) for the two quantum states. We examined these beating in details in Section 3.

In addition, well distinguishable peaks can be observed at about 0.2 PHz, which appeared in both cases. The origin of these peaks has not yet been resolved; it could be the consequence of the coupling between 5s, 5p, 6p and one higher atomic level, which were not included in our model.

As it was mentioned earlier, a small part of the laser beam from the HHG source added about 2% intensity to the pump beam, which could add up to 14% electric field by interference. This beam however propagates together with the attosecond pulse train and consequently has no delay (τ) dependence. The transmission change ΔT is proportional to the square of the transition dipole moment (d) as can be seen from Eq. (1) and (A1) in [10], and consequently it can be expressed as $\Delta T \propto |d(\tau)|^2 + |d_0|^2 + d(\tau)d_0^* + d^*(\tau)d_0$ where the delay dependent $d(\tau)$ is caused by the pump laser field and delay independent d_0 is caused by the weaker laser field from the HHG source. The first term gives the signal one want to measure; the second term is a constant shift and the last two terms are the interference terms. The interference terms are proportional to d_0 giving only 14% contribution to the signal. Furthermore, they are linear with $d(\tau)$ meaning that they give an oscillation with the 0.375

PHz frequency of the laser field, what can be distinguished from the other contributions mentioned above and can be easily Fourier filtered causing no problem in the measurements.

As can be seen in the inset of Fig. 1(a) the laser beam at the Kr gas had a ring structure what fulfilled the 1-mm hole in the gas tube. The XUV beam size was about 0.4 mm and illuminated few inner rings depending on the opening of the aperture for controlling the pump pulse energy. The input slit of the spectrograph, however allowed only a part of the central region into the spectrograph. Along the slit, the XUV beam still saw different laser intensities but they arrived at different part of the CCD. A central band region of the CCD was averaged to get the XUV spectra presented still covering the central range and the first ring. Because the amplitude of the linear beat is proportional with the laser intensity Eq. (5), the effect of the average intensity was measured. For the non-linear beat, the square-average was measured. It made only possible to draw conclusion not about the amplitudes of the linear and the non-linear beat but their present.

4.2.3. Attosecond dynamics of the transient absorption in case of strong ionization

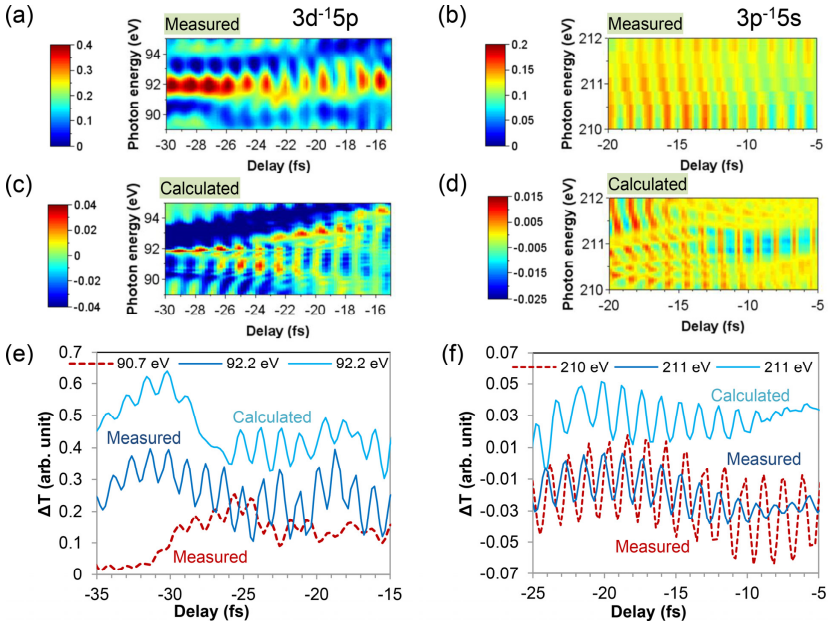

Fig. 6. Attosecond dynamics of the dressed Kr was resolved at laser intensity of 6×10^{14} W/cm^2. The measurements and calculations of (a), (c) $3d^{-1}5p$ and (b), (d) $3p^{-1}5s$ dressed transitions showed the fast transmission change caused by the electric field of the dressing laser pulse beyond the slow change. (e), (f) At certain photon energies, the comparison of the measurements and the calculations shows very good agreements.

To study the transient processes in more detail, a part of the delay range around zero delay of Figs. 4(a) and 4(c) was scanned with a higher temporal resolution of 170 as temporal steps and the delay range when the absorption line start to split was plotted in Figs. 6(a) and 6(b) and compared with the calculations of Fig. 6(c) and 6(d). Here, we aimed to study laser dressing, thus Fourier windows at the 0.75 PHz dressing peak and at the zero-order were applied. Beyond the temporal and spectral patterns recognized earlier, the fast change in the transmission caused by the electric field of the dressing laser pulse appeared in both spectral ranges. The calculations showed much richer temporal and spectral structures that were not possible to resolve with the measurements; however the main structural properties were well resolved in both cases. We would like to highlight the phase shift along the vertical line structures caused by the electric field of the dressing laser pulse, which consequently have a temporal period of 1.3 fs. In Fig. 6(a), a phase shift of about one quarter period (0.7 fs) can be

observed between the two measured periodic structures, just above and below the absorption line at 91.3 eV, which can also be seen in the calculation. A similar shift can be observed at the absorption line of 210.4 eV in Fig. 6(b). At the two photon energies below and above the two absorption lines, the transmission changes were plotted in Figs. 6(e) and 6(f). Both the slow changes and the fast periodic modulations show very good agreement between the measured and the calculated results (dark and light blue solid lines), and additionally, the phase shift between the curves plotted at different photon energies (red dashed lines) are clearly visible.

4.2.4. Attosecond dynamics of the transient absorption in case of weak ionization

As can be seen in Figs. 3(c) and 3(f), when dressing the Kr atoms with a strong laser field of 6 × 10^{14} W/cm^2 the original absorption line of the atoms disappeared completely, and only weak and strongly structured absorption appeared during the time the atoms were illuminated with the laser pulse. Additionally, this induced absorption was extended over a wide spectral range. Much less extended and more prominent absorption changes were predicted by the theory at lower laser intensities as can be seen in Figs. 3(a), 3(b), 3(d) and 3(e). To study this case, we performed measurements at two lower dressing intensities of 4 × 10^{13} W/cm^2 and 8 × 10^{13} W/cm^2. At the former intensity, we observed no visible ionization of the Kr gas, while at the later one, a weak ionization was visible.

To look into the measurements in detail, temporal and spectral windows of interest have been plotted in Figs. 7(a) and 7(c), namely at around 92.4 eV at higher intensity, and at around 210.4 eV at lower intensity. The involved transitions are noted with red dashed arrows in Figs. 7(a) and 7(c). As it can be recognized for both transitions, the phase of dressing (0.75 PHz) transmission modulation shifted at around the absorption lines. Plotting the transmission change separately at nearby photon energy (orange dashed) together with the transmission at the absorption lines (blue) in Figs. 7(b) and 7(d), the phase shift can be well recognized. An interesting phenomenon can be observed in both transitions, namely that the sign of the phase shift changed at about −12 fs and −18 fs delays respectively. In our measurements, we were able to resolve the phase shift of the transmission with accuracy between 300 as and 650 as.

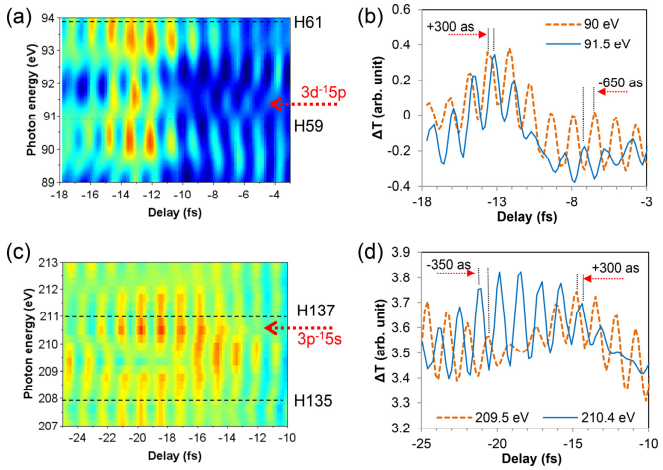

Fig. 7. Attosecond dynamics of the dressed Kr was resolved at laser intensity of (a) 8 × 10^{13} W/cm^2 at 3d^{-1}5p and (c) 4 × 10^{13} W/cm^2 at 3p^{-1}5s transitions. In panels (b) and (d), the delay dependence of the transmission changes were compared at two nearby photon energies.

For further comparison, a larger delay range was also measured and the measurement results were plotted in Figs. 8(b) and 8(d) for both transitions of 3d^{-1}5p and 3p^{-1}5s as noted in the figure. In these measurements, we did not use the Si foil as earlier in Fig. 4, so that the effects of the dressing over 100 eV became also visible. Furthermore, we did not filter out the

zero order as we did in the strong field measurement in Fig. 4. We used here another method to eliminate the shape of the spectrum and harmonic lines, namely, we subtracted the DC part of the delay-dependent signal at every photon-energy and plotted only the AC part.

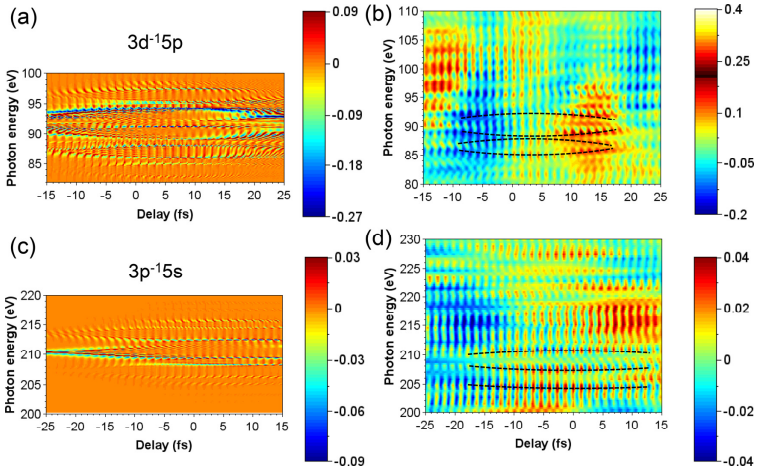

Fig. 8. Attosecond dynamics of the dressed Kr was resolved at laser intensity of 8×10^{13} W/cm^2. The calculations (a), (c) and measurements (b), (d) of (a), (b) $3d^{-1}5p$ and (c), (d) $3p^{-1}5s$ dressed transitions showed the dense periodic change of the transmission caused by the electric field of the dressing laser pulse. The split of the absorption lines and the appearance of the dressed states are highlighted with black dashed lines.

In the left column of Fig. 8, we put the magnified part of the calculations plotted in the same delay ranges as the measurements were made. It can be recognized on the calculated figures that the original absorption lines were split and opened to ± 1 and ± 2 order dressed lines. Additionally, a fast periodic structure was around the dressed lines everywhere with a period of half optical cycle of the dressing laser field (1.34 fs or 0.75 PHz). The split of the absorption lines can be recognized in the measurement too (right column). Furthermore, the higher order (mainly negative order) dressed states caused additional absorptions and spectrally periodic patterns with about 1.5 eV periods. The split of the absorption lines and the new dressed states were highlighted with gray dashed lines in the measured (b) and (d) panels.

For direct comparison, the delay dependence of the XUV transmission was separately plotted in Fig. 9 at few photon energies around the absorption lines. The calculated curves at four dressing laser intensities were plotted with plastic colors and shifted with integers for better visibility. At the two measured intensities, the results (within the narrower delay range of the measurements) were plotted with similar but darker colors and also shifted with half-integers for better visibility.

The measured transmission curves followed the theoretical predictions very well: At 94 eV and 209.5 eV, the dressing laser induced absorption with two characteristic valleys (noted with black arrows) being more prominent at higher intensities and their positions were dependent on the laser intensity. On the measurements, both the laser induced absorption and the presence of the valleys and the mentioned characteristics were observed at the correct delays. Additionally, around zero delay, the theory predicted increasing amplitude of the modulation of 0.75 PHz dressing on increasing intensity, what was also observed. At 210.4 eV, the original absorptions of the Kr atoms were canceled by the laser pulse and even transient gain (larger than 1 transmission) appeared at the characteristic peaks at around –20 fs delay at intensity of 4×10^{13} W/cm^2, what range was anyway measured and plotted in Fig. 7(c). This peak that was well visible at low intensities, almost disappeared at higher intensities both in the theory and the experiments, see Fig. 9(c). Similar transient gains were

theoretically predicted at 94 eV and at about + 20 fs delay at larger laser intensities of 8 × 10^{13} W/cm^2 and 1 × 10^{14} W/cm^2 in Fig. 9(a). Transient gain was also theoretically predicted and experimentally observed in Fig. 6(a)-6(d), where the calculated positive transmission change (red colors) meant larger than 1 transmission or gain.

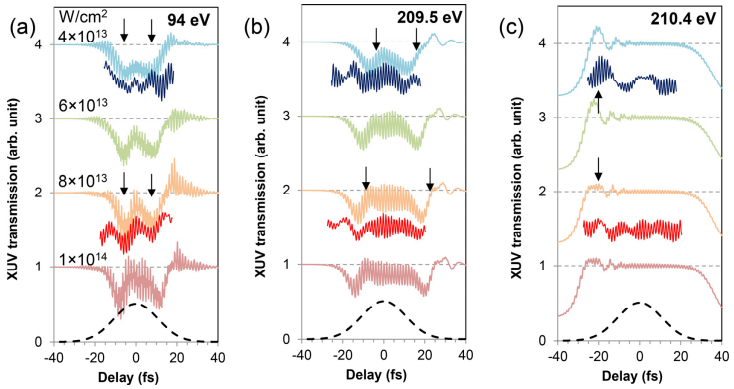

Fig. 9. Attosecond dynamics of the dressed Kr is plotted (light colors) at four laser intensities of the calculation and (dark colors) two intensities of the measurement at few photon energies. For better visibility, the curves were shifted vertically with integers in the case of the calculations and with half-integers in the case of the measurements.

5. Conclusion

By using attosecond pulse trains of HHG and the broad generated spectrum covering the 70 - 230 eV photon energy range, we studied laser dressed krypton atoms by attosecond transient absorption spectroscopy at the two core level transitions $3d^{-1}5p$ and $3p^{-1}5s$, at 91.3 eV and 210.4 eV, respectively. The energy difference of the 5s and 5p levels of Kr (1.52 eV) gave us a unique opportunity for resonantly dressing these levels with the laser pulses of a Ti:sapphire laser system. Therefore, we were able to observe strong dressing effects not only at high laser intensities such as 6 × 10^{14} W/cm^2, but even at about 10 times lower laser intensities of 4 × 10^{13} W/cm^2 and 8 × 10^{13} W/cm^2 too. In the meantime, we modeled the dressing processes with three- and four-level density matrix equations beyond the rotating-wave approximation and compared the experimental and theoretical results. The theory predicted a complex temporal behavior of the transmission change containing delay ranges with transient absorption and with transient gain also in the femtosecond time scale and fast laser field driven temporal oscillations at its second, fourth and sixth harmonic frequencies of 0.75, 1.5 and 2.25 THz. Experimentally we observed the second and fourth harmonics. Furthermore, we observed quantum beats at 0.3 PHz and 2.0 PHz which were attributed to the beating between the $3d_{5/2}$ and $3d_{3/2}$ sub-levels and the $3p_{3/2}$ and $3p_{1/2}$ sublevels, respectively.

Funding

EC 7th Framework Program (grant 284464, Laserlab Europe HIJ-FSU001975); ERC Starting Grant 258603 and the EU-FET-Open 664732 “nuClock”; Spanish Ministry of Economy and Competitiveness “Plan Nacional” (FIS2014-51997-R); Japanese Society for the Promotion of Science “KAKENHI 17H02813”.